ELSEVIER

Journal of Nuclear Materials 265 (1999) 117–123

journal of nuclear materials

Electron energy-loss spectroscopy (EELS) study of oxidation states of Ce and U in pyrochlore and uraninite – natural analogues for Pu- and U-bearing waste forms

Huifang Xu [a,*], Yifeng Wang [b,1]

[a] *Transmission Electron Microscopy Laboratory, Department of Earth and Planetary Sciences, The University of New Mexico, Northrop Hall, Albuquerque, NM 87131-1116, USA*

[b] *Sandia National Laboratories, 115 North Main Street, Carlsbad, NM 88220, USA*

Received 8 June 1998; accepted 8 September 1998

Abstract

EELS based on features of ELNES of M_4 and M_5 edges can provide information regarding oxidation states of Ce and U in proposed host phases of radioactive wastes (e.g., pyrochlore, uraninite, and zirconolite). M_4 and M_5 edges of Ce^{4+} have higher energy-loss than those of Ce^{3+}. Intensity ratio between M_4 and M_5 edges and weak peaks after the M_4 and M_5 edges can be used for quantification of Ce^{3+} and Ce^{4+}. EELS results from an unaltered area of pyrochlore from Inner Mongolia of China shows Ce^{3+} and other rare earth (RE) elements. However, EELS spectrum from the neighboring altered area shows Ce^{4+}, Ba and other RE elements. The oxidation of Ce results in loss of RE elements, U, and daughter product of α-decay, Pb during the alteration of the pyrochlore. However, most RE elements were incorporated in to alteration product, the Ce^{4+}-bearing pyrochlore. EELS spectra from a partially α-recoil damaged uraninite show that the ratio of U^{6+}/U^{4+} is about 2/3. The alteration of uraninite and spent fuel (UO_2) in relatively reducing geological fluid results in the formation of coffinite that is a stable secondary waste form at low temperature.

PACS: 61.14.-x; 61.16.-Bg; 64.70.Kb; 71.23.-k

1. Introduction

Crystalline phases of pyrochlore, zirconolite (a derivative structure of pyrochlore), perovskite, and hollandite that can incorporate a variety of radionuclides (e.g., U^{4+}, U^{6+}, Pu^{3+}, Pu^{4+}, Pu^{6+}, Ba^{2+}, Sr^{2+}, Cs^{+}, Rb^{+}) and neutron absorbers (e.g., Th^{4+} and Gd^{3+}) are considered as stable high-level waste (HLW) forms [1,2]. The radionuclides are initially incorporated in these phases. However, alteration and corrosion processes of the crystalline phases in geological repositories will result in re-distribution of the radionuclides among alteration products and local fluids. The crystalline HLW forms will experience corrosion in geological repositories at elevated temperature. In general, corrosion includes radiation damage, dissolution, and alteration (i.e., solid state chemical and structural modification with fluid as a catalyst). Alteration will change the structure and composition of the host phases, affect oxidation states of radionuclides, and redistribute radionuclides in alteration products and local fluids. Over the long-term, the alteration products containing radionuclides and their fission products become the secondary waste forms, or near-field source. The understanding of detailed properties of the alteration products (i.e., secondary waste form) can permit reliable long-term performance prediction of crystalline HLW [1,2]. Understanding the valence states of multi-valence cations (U^{4+}, U^{6+}, Pu^{3+}, Pu^{4+}, and Pu^{6+}) in host phases and their alteration products is also

* Corresponding author. Tel.: +1-505 277 7536; fax: +1-505 277 8843; e-mail: hfxu@unm.edu.

[1] E-mail: ywang@nwer.sandia.gov.

0022-3115/99/$ – see front matter
PII: S0022-3115(98)00566-2

important to evaluate the long-term corrosion reactions of ceramic waste forms, such as Synroc [3].

Laboratory corrosion tests have been conducted for HLW forms. Transmission electron microscopy (TEM) and electron energy-loss spectroscopy (EELS) techniques are also used for characterization of HLW forms and corrosion products [4]. The secondary phases formed during leaching experiments of Synroc are precipitates of TiO_2 polymorphs (anatase and brookite) [5,6]. However, all those tests can only determine the short-term (hours to years) behavior of waste forms. In addition, those tests have been conducted under far-from-equilibrium conditions, in order to obtain measurable dissolution rates for extremely sluggish corrosion processes; as a consequence, the formation of secondary minerals is inevitably eliminated in the tests. Apparently, laboratory experiments are unable to simulate actual waste alteration processes in geologic repositories over a time scale of 10 000–100 000 years. The alternative is to use natural analogues, that is, to obtain relevant long-term information from naturally occurring mineral phases that have already experienced alterations on a geologic time scale in natural environments. Understanding the behavior of U and Ce during the alteration directly impacts the long-term performance evaluation of the crystalline HLW forms. Natural Ce- and U-bearing minerals and their alteration products can be used as 'natural analogues' to study long-term alteration and corrosion behavior of the crystalline HLW form. The chemical species of Ce^{3+}, Ce^{4+}, U^{4+}, and U^{6+} in those minerals can be used as chemical analogues for Pu^{3+}, Pu^{4+}, and Pu^{6+} [3].

High-resolution TEM (HRTEM) and associated EELS are powerful tools for studying microstructures (or textures), oxidation states, and chemical bonding of materials at the nanometer scale. Field-emission gun (FEG) with highly coherent and strong electron beam source can provide high-energy resolution (within 1 eV) electron energy-loss spectra from nanometer-scale areas. High-energy resolution EELS spectra will provide more information about the ions and their neighboring environment.

2. EELS and associated HRTEM

In a transmission electron microscope, high-energy electrons that have been elastically scattered by the specimen may be used for imaging and diffraction from specific areas of the specimen. This provides important structural information about the specimen. The high spatial resolution offered by HRTEM has been used for studying structures and microstructures (or textures) at the atomic scale.

The incident high-energy electrons also undergo inelastic interaction with the specimen that can provide further information about chemistry and electronic structures of the specimen [7]. This has given rise to analytical electron microscopy (AEM) based on X-ray energy-dispersive spectroscopy (EDS) and electron energy-loss spectroscopy (EELS) in the TEM. EELS can provide valuable information about the specimen under study, such as quantitative chemical analysis, oxidation states, coordination, crystallinity, and chemical bonding types, based on the electron energy-loss near-edge structure (ELNES) of a core-loss edge [7–10]. EELS and ELNES are electron analogues for XAS and XANES. The integrated study of HRTEM and EELS can provide information regarding microstructure, micro-chemistry of mineral reactions at the nanometer scale. Parallel EELS (PEELS) developed commercially by Gatan makes it possible to acquire a spectrum within 2–5 s, far more rapidly than that with serial EELS spectrometers [11]. Electron beam-induced radiation damage is thereby minimized.

An EELS spectrum displays the electron intensity as a function of energy-loss and can be divided in to several regions. The intense zero-loss peak (ZLP) results from transmitted electrons that undergo elastic and quasi–elastic interactions. The electron energy spread, microscope high voltage stability, and the energy resolution of the spectrometer determine the width of ZLP. These factors also determine the energy resolution of EELS spectra. Highly coherent electron source of field-emission gun (FEG) displays sharper ZLP than thermoionic sources do. The region following the ZLP and extending to energy-loss of about 50 eV is called low-loss region [8,11]. This region is dominated by plasmons that results from collective excitations of valence electrons. The region may provide information about dielectric function, valence electron densities, and specimen thickness. High energy-loss (i.e., core-loss) edges superimposed on a decreasing background from lower energy-loss processes result from the transition of core electrons to unoccupied states in the conduction band. The core-loss edges usually take the shape of a step. The sudden rise in intensity represents ionization threshold (Fig. 1). Notations for the core-loss edges are same as that for spectroscopy notations. For instance, in Fig. 1, Fe $L_{2,3}$ edges result from the transition from the 2p core levels. ELNES includes the region from edge onset to about 30–50 eV above the edge onset. EELS can provide chemical information for all elements except H.

3. Samples and experiments

The pyrochlore sample $(Ca, Ce^{3+})(Ti, Nb)O_{7-x}(HO)_x$ is from a rare earth (RE) element ore deposit of Inner Mongolia of China. Hydrothermal alteration involves the formation of Fe^{3+}-rich amphibole, Fe^{3+}-rich pyroxene, and Ba–Ce-carbonates [12]. The uraninite

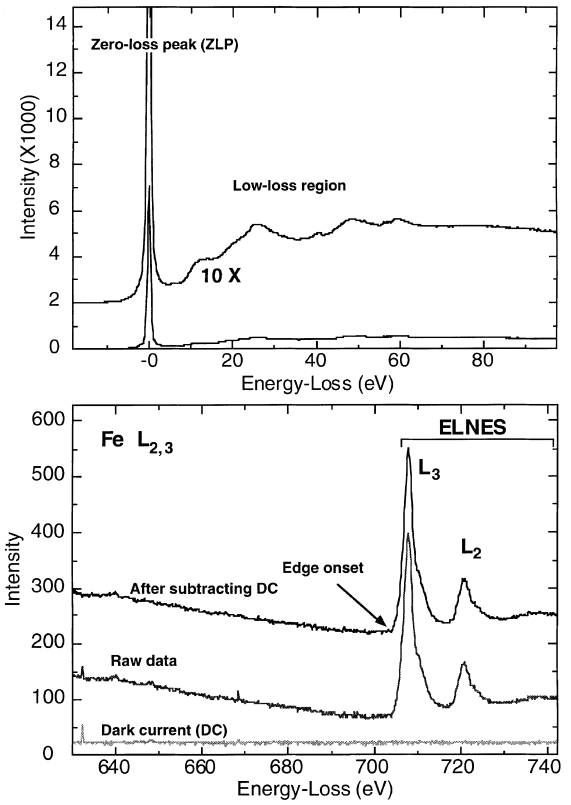

Fig. 1. EELS spectra showing zero-loss peak (ZLP) and low-loss region (upper) and a core-loss edge (lower) from a mineral ilmenite ($FeTiO_3$).

sample is from Port Radium Mine of Northwest Territories, Canada. Quartz veins and fine (about 0.1 mm width) coffinite ($U[SiO_4] \cdot nH_2O$) veins that are alteration products of the uraninite cut through the uraninite. All HRTEM and EDS results were carried out with a JEOL 2010 HRTEM. Point-to-point resolution of the HRTEM is 0.19 nm. All EELS results were carried out with a Philips 420ST FEG TEM and Gatan PEELS system. Energy resolution of the PEELS system measured from ZLP is about 0.9 eV.

4. Results and discussion

4.1. Ce^{3+}- and Ce^{4+}-bearing phases

ELNES spectra of Ce-M_5 and Ce-M_4 edges from several Ce-oxides show that post-edge peaks are associated with Ce^{4+} (Fig. 2). The peak positions of M_5 and M_4 edges of Ce^{4+} shift to higher energy-loss by 1.3 and 1.4 eV, respectively, with respect to those of Ce^{3+} (Fig. 2). The intensity ratio between M_5 and M_4 edges increases as the ratio of $Ce^{3+}/(Ce^{4+} + Ce^{3+})$ increases in

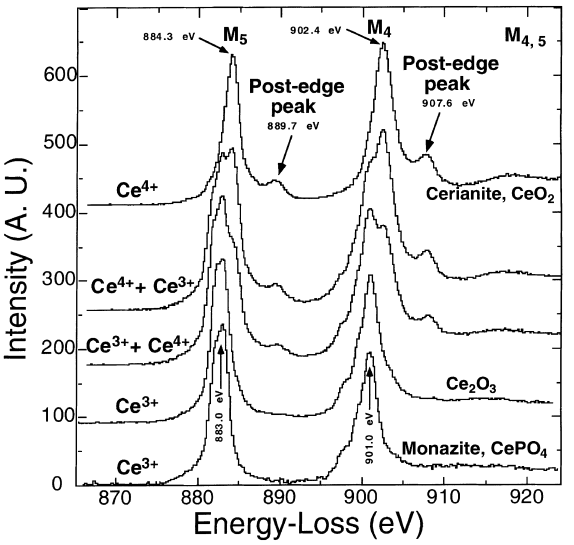

Fig. 2. EELS spectra of CeO_2–Ce_2O_3 system showing ELNES of Ce M_5 and M_4 edges. Post-edge peaks of M_5 and M_4 edges characterize Ce^{4+}. A spectrum from monazite (Ce^{3+}) is also illustrated for comparison.

the Ce-bearing oxides with fluorite or modified-fluorite structures (Fig. 2). The intensity ratios between M_5 and M_4 edges are 1.12 and 0.75 for Ce^{4+} and Ce^{3+}, respectively. However, the intensity of post-edge peaks decreases as the ratio of $Ce^{3+}/(Ce^{4+} + Ce^{3+})$ increases. ELNES of oxygen K-edge also changes as the ratio of $Ce^{3+}/(Ce^{4+} + Ce^{3+})$ changes in the oxides (Fig. 3). The pre-edge peak of oxygen characterizes oxygen bonding with Ce^{4+}. Spectra from both the O–K edge, and Ce-M_5 and Ce-M_4 edges provide information about the oxidation states of Ce. The intensity ratio between pre-edge peak and K-edge peak of oxygen, and the intensity ratio

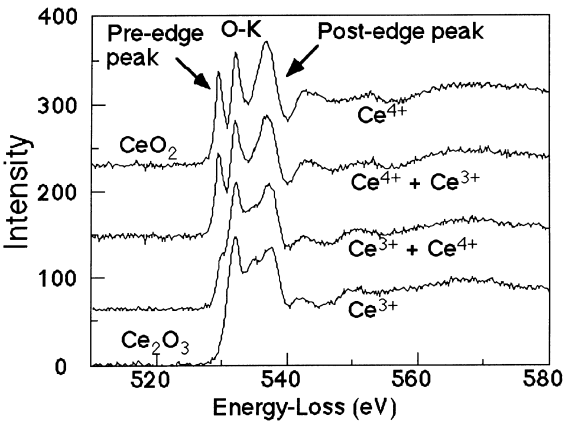

Fig. 3. EELS spectra CeO_2–Ce_2O_3 system showing ELNES of oxygen K-edge. Pre-edge peaks of O–K characterize oxygen bonding with Ce^{4+}.

between the post-edge peak of Ce M_5 and M_4-edge peaks can be also used for quantification of $Ce^{3+}/(Ce^{4+} + Ce^{3+})$ ratio and redox ability of the Ce-bearing oxides. EELS has been successfully applied to the characterization of oxidation states of Ce, U, and Pu in Synroc and glass HLW forms [4].

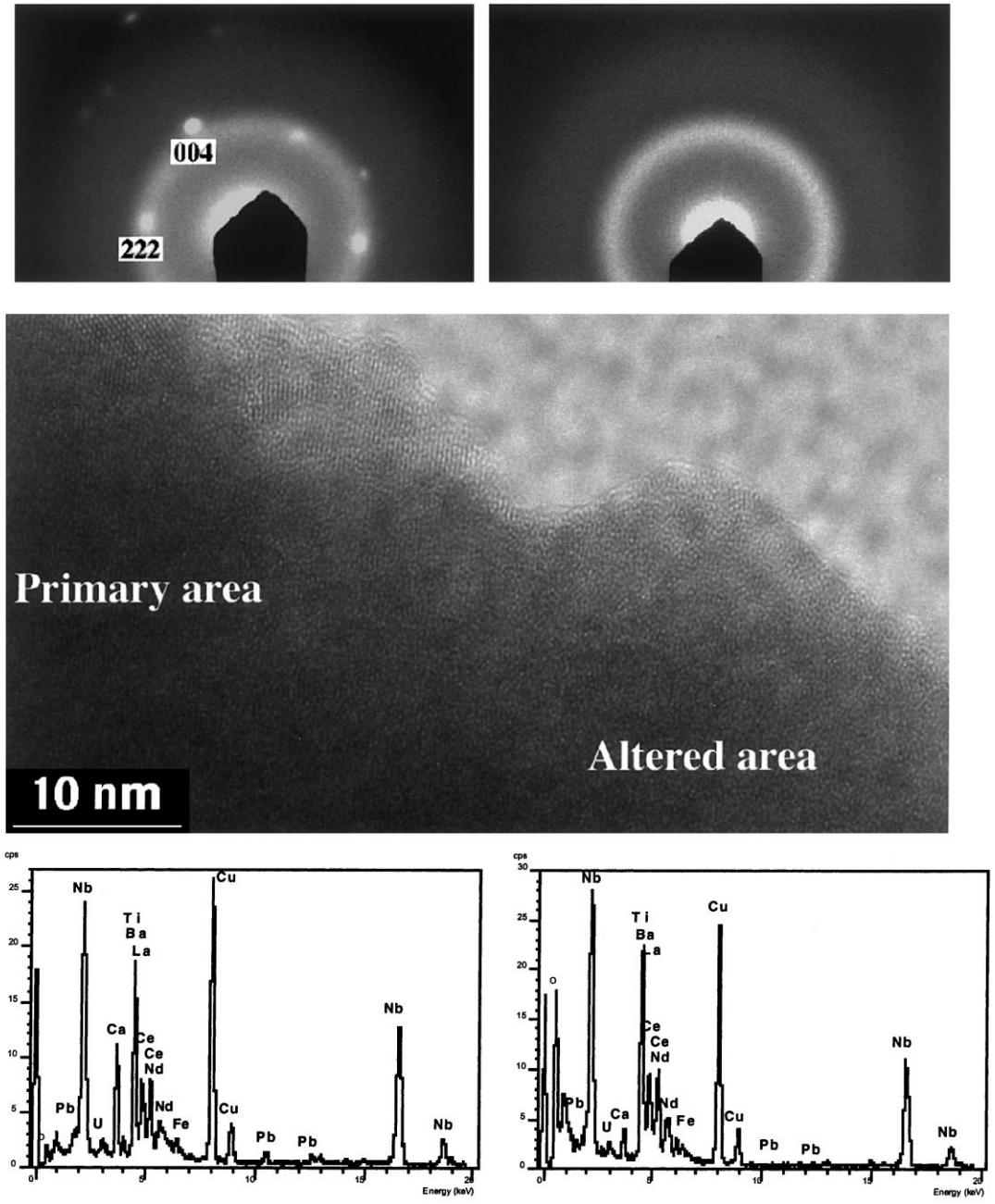

Fig. 4. SAED patterns (top) from primary (Ca-rich) area (partially metamict state) and an altered (Ca-poor, metamict state) area in an pyrochlore; HRTEM image (middle) showing the boundary between the metamict and partially metamict pyrochlore; EDS spectra (bottom) from areas across the boundary. Diffuse rings in the SAED patterns characterize aperiodic arrangement of polyhedra with average size of 3 Å in the α-recoil damaged pyrochlore. The EDS spectra show that the primary area (left) is relatively rich in Ca with respect to the altered area. However, the EDS spectra are unable to resolve Ti, Ba, and REE at 120 eV energy resolution. Cu peaks result from Cu-grids holding the specimen.

HRTEM and AEM results from a partially metamict pyrochlore (REE, Ca) (Nb, Ti)O_4 and its alteration product (Ba, Ca, Ce^{4+})$_2$(Ti, Nb)$_2O_{7-x}(OH)_x$ show that the alteration product is metamict and relatively poor in Ca (Fig. 4). EELS spectra show that the altered area contains Ba, Ce^{4+} and other REE elements (Fig. 5). The EELS spectra clearly resolve Ba and all REE in the pyrochlore. The peak positions of M_5 and M_4 edges of Ce in the alteration product shift to higher energy-loss by 1.25 eV with respect to the Ce in the primary phase (Figs. 5 and 6). The intensity ratios between M_5 and M_4 edges based on second difference EELS spectra (Fig. 6) are 1.06 and 0.77, respectively, for the alteration product and the primary phase. If we approximately assume a linear relationship between the intensity ratio between M_5 and M_4 edges and the ratio of $Ce^{3+}/(Ce^{4+} + Ce^{3+})$, it can be calculated that the $Ce^{3+}/(Ce^{4+} + Ce^{3+})$ ratios for primary phase and alteration product are 0.95 and 0.16, respectively.

The alteration associated with the formation of Fe^{3+}-rich amphibole indicates that Ca- and Ba-bearing oxidizing fluid is responsible for the alteration. The alteration in oxidizing environment results in loss of RE elements, U and Pb. The peaks of low contents of Gd and Eu do not show clearly, because of the loss of Gd, Eu and other REE during the alteration. The reaction of the pyrochlore alteration may be expressed as:

$$(Ca, Ce^{3+}, REE^{3+})_2(Ti, Nb)_2O_{7-x}(OH)_x + O_2 + Ba^{2+} + H^+ \rightarrow (Ba, Ca, Ce^{4+}, REE^{3+})_2(Ti, Nb)_2O_{7-y}(OH)_y + REE^{3+} + Ce^{4+} + Ca^{2+} + H_2O.$$

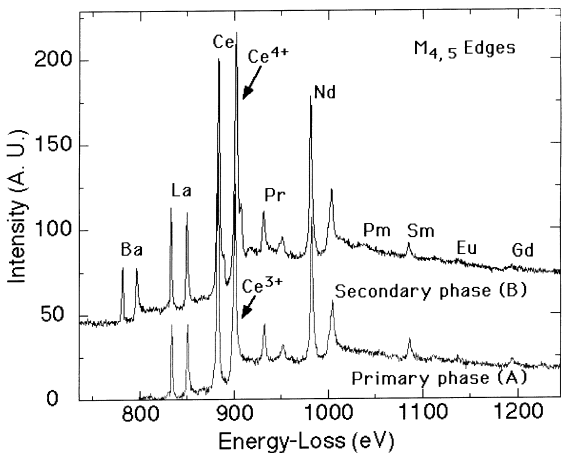

Fig. 5. EELS spectra from primary (Ca-rich) pyrochlore (A) and its alteration product, metamict pyrochlore (B). Spectrum (A) shows Ce^{3+} and other RE elements. However, spectrum (B) shows Ba, Ce^{4+}, and other RE elements. The intensity ratio between M_5 and M_4 edges can be used for quantifying Ce^{4+}/Ce^{3+} ratio. Low content of Gd and Eu in the alteration product shows the loss of RE elements during the oxidization of Ce in oxidizing fluid.

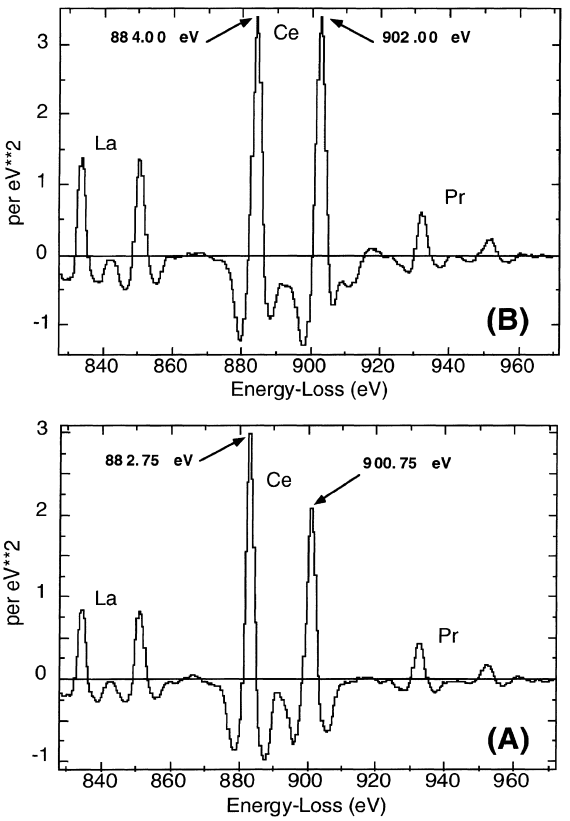

Fig. 6. Second difference EELS spectra from primary (Ca-rich) pyrochlore (A) and its alteration product, metamict pyrochlore (B) showing intensities of M_5 and M_4 edges of Ce. The intensity ratio between M_5 and M_4 edges can be used for quantifying Ce^{4+} and Ce^{3+}.

(REE = rare earth element.) The oxidation of Ce^{3+} (analogue for Pu^{3+}) results is the loss of Ce, U, and Pb. If Pu is loaded in the pyrochlore in the form of Pu^{4+}, the host phase of Pu^{4+}-bearing pyrochlore will be stable even in relatively oxidizing environments.

4.2. U^{4+}- and U^{6+}-bearing phases

Uraninite can be used as a natural analogue for spent fuel (UO_2). Alteration reaction of uraninite may provide information regarding long-term corrosion reactions of spent fuel in a geological repository. Uraninite may react with silica and for coffinite in relatively reducing environment. Thermodynamic calculation for the coffinitization of uraninite (UO_{2+x}) shows that the reaction that occurs only at low temperature ($T < 130$°C) depends on uraninite composition (presence of U^{6+}), oxygen fugacity, and molality of aqueous silica (Fig. 7). TEM results show the uraninite (UO_{2+x}) and its alteration product coffinite ($U[SiO_4] \cdot nH_2O$, or $U[SiO_4]$).

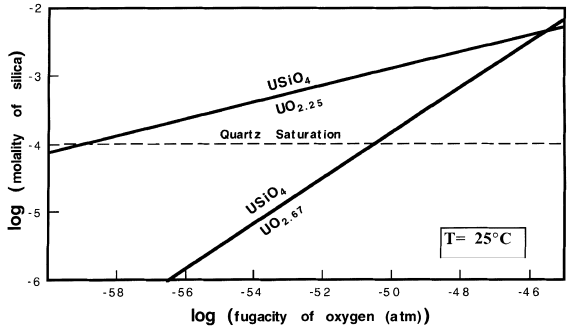

Fig. 7. Equilibrium silica concentration in the coffinitization of UO_{2+x} as functions of oxygen fugacity and oxidation state of U in uraninite.

HRTEM results show α-recoil damage, lattice distortion, and low-angle boundaries among neighboring uraninite domains (Fig. 8). EDS spectrum shows U and its daughter product of α-decay, Pb. EELS spectrum from the uraninite indicate the ratio of U^{6+}/U^{4+} is about 2/3. However, the coffinite that is dominated by U^{4+} contains less Pb than the neighboring uraninite does (Fig. 8). The chemical formula of the uraninite can be expressed as $(U^{4+}_{0.54}, U^{6+}_{0.36}, Pb^{2+}_{0.1})O_{2.26}$. In general, the reaction for coffinitization of natural uraninite with both U^{4+} and U^{6+} can be simplified as

$$UO_{2+x} + SiO_{2,aq} \rightarrow USiO_4 + 0.5x\, O_2.$$

It is proposed that Pb, the fission product of U, was leached out from the uraninite during the reaction from uraninite into coffinite. Spect fuel (UO_2) will transform into uraninite, $(U^{4+}_{1-x}, U^{6+}_{x})O_{2+x}$, because UO_2 is unstable with respect to uraninite even in reducing geological environment. Based on the observed results, the alteration reaction of spent fuel (UO_2) in relatively reducing and silica-bearing fluid may be written as

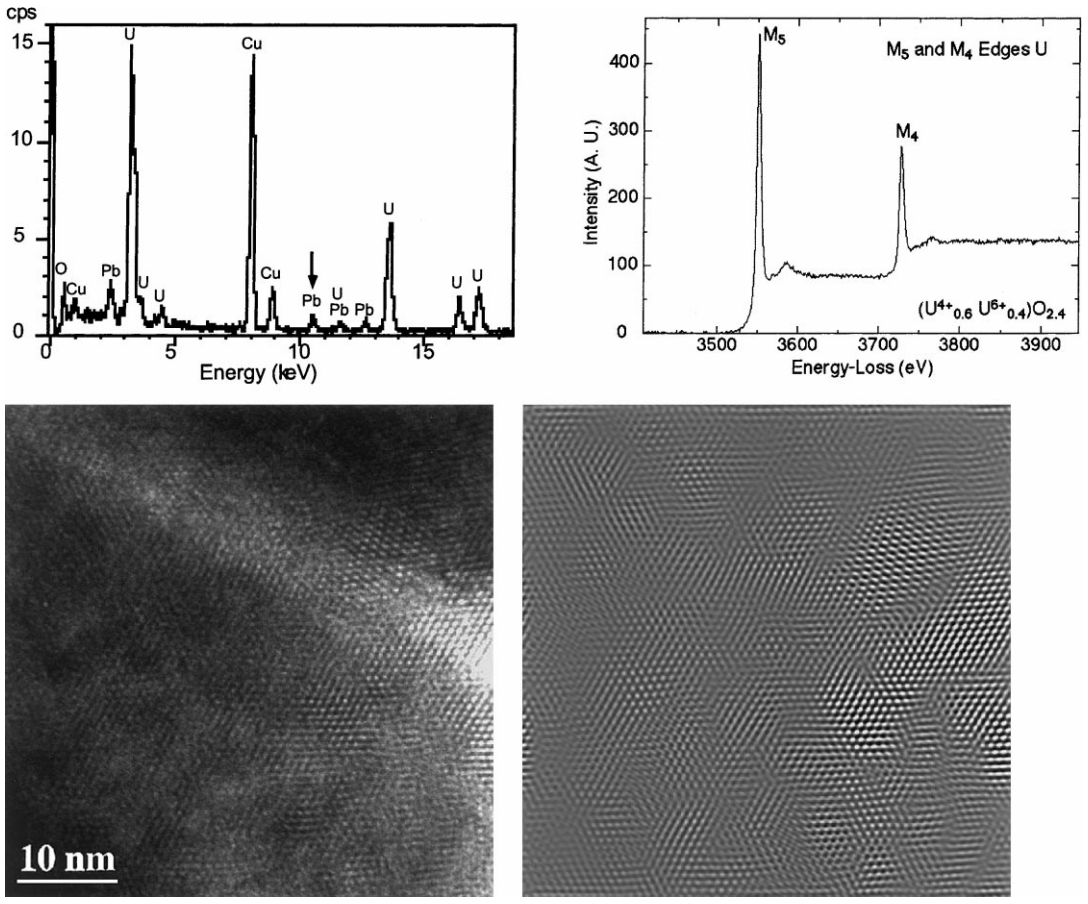

Fig. 8. EDS spectrum (top left) showing U and its fission product Pb in a uraninite crystal; HRTEM image (lower left) and its spatially filtered image (lower right) showing α-recoil damage, lattice distortion, and low-angle boundaries between the neighboring uraninite domains (or islands); EELS spectrum (top right) showing M_5 and M_4 edges of U (used for characterization of U^{6+}/U^{4+} ratio in the uraninite). Cu peaks result from Cu-grid holding the specimen.

$U^{4+}O_2 + yO_2 + ySiO_{2,aq} \rightarrow (U^{4+}_{1-3y}, U^{6+}_{2y})O_2 + yU^{4+}SiO_4$.

The phase $USiO_4$ (coffinite) is a secondary waste form that can also immobilize U released from uraninite during alteration. The reaction may also occur in spent fuel in geological repository. The α-recoil damaged area with low-grain boundaries in the uraninite may accelerate the diffusion of U in the crystal. If the alteration occurs in oxidizing environment, e.g., weathering in silica bearing fluid, U may form U-hydro-silicates, such as: soddyite $[(U^{6+}O_2)_2SiO_4 \cdot 2H_2O]$ and haiweeite $[Ca(U^{6+}O_2)_2Si_6O_{15} \cdot 5H_2O]$.

5. Conclusion

EELS and associate TEM techniques can provide oxidation states of Ce and U at the nanometer scale. The integrated EELS and TEM results can provide us information about alteration mechanisms of HLW ceramic forms (e.g., pyrochlore) and spent fuel. The alteration of pyrochlore in relatively oxidizing geological fluid results in oxidation of Ce and loss of U, Pb, Ce, and other RE elements. The alteration of spent fuel in geological repository may result in the oxidation of UO_2 and formation of $USiO_4$ (coffinite) even in relatively reducing fluid. The coffinite phase (secondary waste form) can also immobilize U. The integrated EELS and TEM study of natural analogues provides long-term reaction processes of nuclear waste in geological repository at the nanometer scale.

Acknowledgements

This work is based upon research conducted at the Transmission Electron Microscopy Laboratory in the Department of Earth and Planetary Sciences of the University of New Mexico, which is partially supported by NSF, NASA, and State of New Mexico. EELS data were collected in the Center for High Resolution Electron Microscopy of Arizona State University. The authors thank Dr L. Garvie for assistance in collecting EELS data.

References

[1] R.G. Dosch, T.J. Headley, C.J. Northrup, P.F. Hlava, Sandia National Laboratories Report, Sandia 82-2980, 1982, p. 84.
[2] A.E. Ringwood, S.E. Kesson, K.D. Reeve, D.M. Levins, E.J. Ramm, in: W. Lutze, R.C. Ewing (Eds.), Radioactive Waste Forms for the Future, North-Holland, Amsterdam, 1988, p. 233.
[3] E.R. Vance, MRS Bulletin, vol. XIX, 1994, p. 28.
[4] J.A. Fortner, E.C. Buck, A.J.G. Ellison, J.K. Bates, Ultramicroscopy 67 (1997) 77.
[5] K.L. Smith, M. Colella, M.C. Thorogoog, M.G. Blackford, G.R. Lumpkin, K.P. Hart, K. Prince, E. Loi, A. Jostson, in: W.J. Gray, I.R. Triay (Eds.), Scientific Basis for Nuclear Waste Management, vol. 20, Mater. Res. Soc. Proc., vol. 465, Pittsburgh, PA, 1997, pp. 349–354.
[6] K.L. Smith, M.G. Blackford, G.R. Lumpkin, K.P. Hart, B.J. Robinson, in: W.M. Murphy, D.A. Knecht (Eds.), Scientific Basis for Nuclear Waste Management, vol. 19, Mater. Res. Soc. Proc., vol. 412, Pittsburgh, PA, 1996, pp. 313–319.
[7] J.C.H. Spence, in: P.R. Buseck, J.M. Cowley, L. Eyring (Eds.), High-Resolution Transmission Electron Microscopy and Associated Techniques, Oxford University, New York, 1988, pp. 190–243.
[8] L.A.J. Garvie, A.J. Craven, R. Brydson, Am. Mineral. 79 (1994) 411.
[9] R. Brydson, H. Sauer, W. Engel, in: M.M. Disko, C.C. Ahn, B. Fultz (Eds.), Transmission Electron Energy Loss Spectroscopy in Materials Science, The Minerals, Metals and Materials Society, Warrendale, Illinois, 1992, p. 131.
[10] H. Xu, L.A.J. Garvie, Abstracts with Programs of Geological Society of America Annual Meeting, Salt Lake City, 1997, p. 400.
[11] R.F. Egerton, Electron Energy-loss Spectroscopy in the Electron Microscope, Plenum, New York, 1996, p. 48.
[12] CAS-IG (Chinese Academy of Science), Geochemistry of Baiyun Obo REE Ore Deposits, Science Press, Bejing, 1988, p. 550 (in Chinese).